STABILIZING EFFECT OF LONGITUDINAL WALL OSCILLATION ON 2D CHANNEL FLOW

Takashi Atobe
Japan Aerospace Exploration Agency
atobe.takashi@jaxa.jp

Keywords: *Channel Flow, Wall-Oscillation, Stability, Floquet, DNS*

Abstract

The present study investigates a stabilizing effect of longitudinal wall-oscillation on two dimensional channel flow by the Floquet theory. To apply this theory to the present periodic flow, a time-dependent Orr-Sommerfeld equation is discritized using the collocation points. The velocity profile needed in this analysis is calculated by superposition of the plane Poiseuille flow and the Stokes layer because of the linearity of the governing equation. In this study, the Reynolds number, which is defined by maximum mean-flow velocity and a half width between the two walls, is fixed to 10,000 that corresponds to the turbulent state of usual channel flow. When the remaining two parameters, frequency and amplitude of the wall-oscillation, are changed parametrically, it is found that on the parameter space the stable region exists even under the supercritical condition. The direct numerical simulation (DNS) also carried out to validate this feature. DNS demonstrates that the transitional period to the fully turbulent state is longer or shorter compared with non-oscillating case depending on the parameters mentioned above. The comparison of the results obtained the Floquet analysis with DNS shows that the stable region in the Floquet analysis roughly coincides with the region of slow transition.

1 Introduction

Drag reduction is one of the important issue on the public transport system. For the aircraft, the account of skin friction in the total drag is about 50%. Thus many researchers focused on how to reduce the skin friction. Some people tried by passive control, as the wavy walls or roughness surface[1,2]. On the other hand, as active control, wavy walls, vibrating walls, or suction/blowing walls were examined[3-6].

In these studies, it seems that the oscillating wall is one of the candidate for realizing low friction systems. Jung et al.[7] firstly pointed out that spanwise wall-oscillation of the two dimensional channel flow can reduce the wall shear stress for a turbulent channel flow. Succeeded study by Quadrio and Ricco[8] numerically demonstrated the friction-drag reduction of 44.7% and also estimated the net energy saving of 7.3%.

From a different viewpoint, there are some studies which investigated a simplified flow field[9,10]. Basic idea of these studies is combination of the plane Poiseuille flow with the oscillating Stokes layer. The strong point of this strategy is that both flow field are described as exact solutions of a linear equation derived from the Navier-Stokes equation. Since there are many theoretical and numerical investigation have revealed its essential features for the plane Poiseuille flow[11,12], it seems that this approach using the combination of these two flows is useful to understand the characteristics of the stability. However, treatment of the periodicity of the flow is an obstacle.

In general, the stability of the flow, such as the boundary layer flow, can be described by the Orr-Sommerfeld (O-S) equation which is derived from the Navier-stokes equation. But on the unsteady system, the differential term with respect to time remains in the O-S equation. Although the Floquet theory is a strong tool for stability analysis of such a periodic systems, it is difficult to directory apply the Floquet theory on this time-dependent O-S equation. In order to avoid this difficulty, author adopts a discretization into the time-dependent O-S equation. Then this discretization can rewrite it as a simple periodic differential equation and allows us to use of the Floquet analysis.

The purpose of the present paper is to investigate the stability of the wall-oscillating channel flow using the Floquet analysis. Also, a DNS is carried out in order to confirm the results obtained by the stability analysis.

In Section 2, the modified channel flow dealt here is explained. In Section 3, a time-dependent Orr-Sommerfeld equation and its discritization are explained, and a methodology linear stability analysis based on the Floquet analysis is described. Then in Section 4, another approach, namely DNS study is demonstrated. Finally conclusions are given in Section 4.

2 Modified Channel Flow

2.1 Linear Combination

A schematic view of the modified channel flow investigated are shown in Fig.1. Here, Ω and U_w are frequency and amplitude of the longitudinal wall-oscillation. Thus, parameters describing this system are Ω, U_w, and the Reynolds number defined as $Re \equiv h\ U_{\max}/\ \nu$, where $U_{\max}$ is the maximum value of the mean flow, ν the kinematic viscosity and h a half distance between two walls. In the present study, Re is fixed as 10,000, which is a supercritical condition, for convenience.

The coordinate system of (x,y,z) corresponding to the physical space is taken for x in the streamwise direction, y in the direction normal to the wall, z in the spanwise direction. As mentioned before, the modified flow dealt here can be thought as a superposition of the exact solutions of a linear government equation as the follows,

$$\frac{\partial U}{\partial t} - \nu\left(\frac{\partial^2 U}{\partial y^2} + \frac{\partial^2 U}{\partial z^2}\right) = -\frac{1}{\rho}\frac{\partial p}{\partial x}, \qquad (1)$$

here ρ is the dencity. This equation is derived from the incompressible Navier-Stokes equation under the parallel flow assumption. In this context, the flow can be represented as $U=U(U(y,t),0,0)$, and $U(y,t)$ is,

$$U(y,t) = 1 - y^2 + U_w \operatorname{Re}\left[\frac{\cosh(\kappa y)}{\cosh(\kappa)}\right]\exp(i\Omega t) \qquad (2)$$

here, $\kappa = \sqrt{\Omega/2\nu}$, and i denotes the imaginary unit. The former part of Eq.(2) is contribution of the plane Poiseuille flow, and the latter is the Stokes layer. In the Floquet analysis, Eq.(2) is used as the base flow.

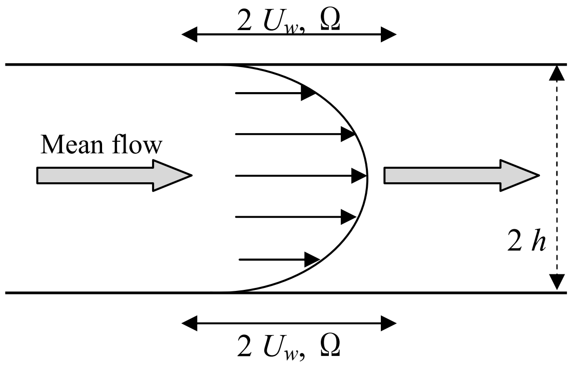

Fig.1 Schematic view of the modified channel flow. Ω and U_w are frequency and amplitude of the longitudinal wall-oscillation.

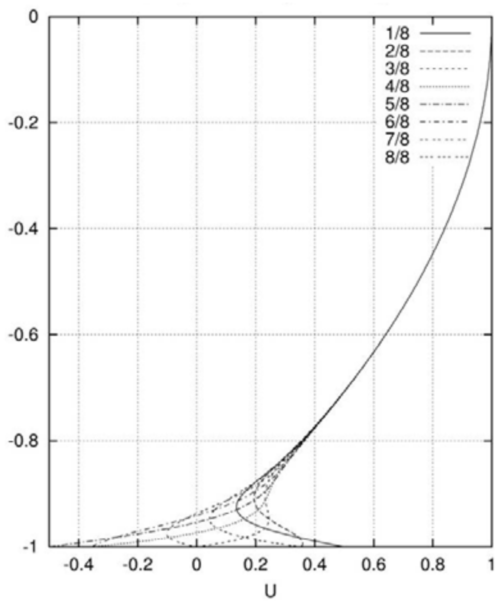

Fig. 2 Velocity profiles at some instances.

2.2 Velocity Profiles

Figure 2 shows a typical velocity profiles at each 1/8 period of the wall-oscillation. Because of the symmetry, the only lower half is shown. In this case, U_w is set to 0.5.

3 Floquet Analysis

3.1 Time-Dependent Orr-Sommerfeld equation

When the flow field is described by the base flow U and the small disturbance $\boldsymbol{u}$ and p, the linearized disturbance equation for $\boldsymbol{u}$ can be derived from the Navier-Stokes equation as the follows.

$$\frac{\partial \boldsymbol{u}}{\partial t} + (\boldsymbol{U}\cdot\mathrm{grad})\boldsymbol{u} + (\boldsymbol{u}\cdot\mathrm{grad})\boldsymbol{U} = -\frac{1}{\rho}\mathrm{grad}\, p + \nu\nabla^2\boldsymbol{u} \tag{3}$$

Now, we assume that the small disturbance can be described as a modal plane wave,

$$\boldsymbol{u}(x,y,z,t) = \hat{\boldsymbol{u}}(y,t)\exp[i(k_x x + k_z z)] \tag{4}$$

here $\boldsymbol{u}$=$\boldsymbol{u}(u,v,w)$, and k_x, k_z are real wave number in x, z direction, respectively. Substituting Eq.(4) into Eq.(3) with the equation of continuity, we obtain time-dependent Orr-sommerfeld equation, which takes the form of

$$\begin{aligned}&[(\frac{\partial}{\partial t} + ik_x U(y,t))(D^2 - k_x{}^2 - k_z{}^2) - ik_x D^2 U(y,t)]\hat{v}(y,t)\\ &= \frac{1}{R}(D^2 - k_x{}^2 - k_z{}^2)^2\hat{v}(y,t)\end{aligned} \tag{5}$$

where D is the differential operator in y direction.

3.2 Flouet Exponents

If Eq.(5) can be rewritten as the form,

$$\frac{\partial}{\partial t}\hat{v}(y,t) = G(y,t)\hat{v}(y,t) \tag{6}$$

because of the periodicity of function G, we can expect from the Floquet theory that the solution of Eq.(6) can be described as the follows,

$$\hat{v}_i(y,t) = e^{\mu_i t}\phi_i(y,t) \tag{7}$$

Here $\phi_i(y,t)$ is a periodic function with the period T, and μ_i is a complex number called as Floquet exponents. If the real part of μ_i is positive, the system should be unstable.

Thus, in order to rewrite Eq.(5) as the form of Eq.(6), the Chebyshev spectral collocation method is employed. For this, Gauss-Lobatto scheme is adopted for the collocation points,

$$y_j = \cos\frac{\pi j}{N+1}, (j = 0,1,2,\cdots,N) \tag{8}$$

Then, Eq.(5) can be rewritten as the follows,

$$(D_{ij}^{(2)} - k_x{}^2 - k_z{}^2)\frac{d}{dt}\begin{pmatrix}\hat{v}(y_0,t)\\ \hat{v}(y_1,t)\\ \vdots\\ \hat{v}(y_N,t)\end{pmatrix} = g_{ij}\begin{pmatrix}\hat{v}(y_0,t)\\ \hat{v}(y_1,t)\\ \vdots\\ \hat{v}(y_N,t)\end{pmatrix} \tag{9}$$

where $D_{ij}{}^{(2)}$ is the differential matrix of the order (N+1) x (N+1). If the inverse matrix of ($D_{ij}{}^{(2)}$ - $k_x{}^2$ -$k_z{}^2$) exists, Eq.(9) can be written in,

$$\frac{d}{dt}\hat{v}(y_j,t) = G_{ij}\hat{v}(y_j,t) \tag{10}$$

When the function $\hat{v}$ is expanded by N+1, Eq.(9) is written in the follows.

$$\frac{d}{dt}\begin{pmatrix}\hat{v}_0(y_0,t)\ldots\hat{v}_N(y_0,t)\\ \hat{v}_0(y_1,t)\ldots\hat{v}_N(y_1,t)\\ \vdots \quad \vdots \quad \vdots\\ \hat{v}_0(y_N,t)\ldots\hat{v}_N(y_N,t)\end{pmatrix} = G_{ij}\begin{pmatrix}\hat{v}_0(y_0,t)\ldots\hat{v}_N(y_0,t)\\ \hat{v}_0(y_1,t)\ldots\hat{v}_N(y_1,t)\\ \vdots \quad \vdots \quad \vdots\\ \hat{v}_0(y_N,t)\ldots\hat{v}_N(y_N,t)\end{pmatrix} \tag{11}$$

If Eq.(11) is simply described as,

$$\frac{d}{dt}F(t) = G(t)F(t) \quad (12)$$

from the Floquet theory, we can expect that the solution of Eq.(12) have the form of,

$$F(t) = e^{Qt}\Phi(t) \quad (13)$$

Here $\Phi(t)$ is an arbitrary periodic function with the period T, and Q consists of $(N+1)$ Floquet exponents. Because of the character of the periodic function $\Phi(t)$,

$$F(0) = \Phi(0) \equiv I \quad (14)$$

Thus,

$$F(T) = e^{QT}\Phi(T) = e^{QT} \quad (15)$$

Therefore, the Floquet exponents are obtained as the follows.

$$Q = \frac{1}{T}\ln F \quad (16)$$

When the eigenvalues of the matrix Q denote as μ_i and the eigenvalues of F as σ_i, we can obtain the Floquet exponents in the form of,

$$\mu_i = \frac{1}{T}\ln\sigma_i \quad (17)$$

Thus, if we know the matrix F, the Floquet exponents are obtained from Eq.(17). In general, the matrix F can be numerically obtained by the integration of Eq.(12) during the period T. In the present study, the Cranc-Nicorson method is employed for this process.

3.3 Results

Substituting velocity profiles shown as Fig. 2 into U in Eq.(5), the time-integration of Eq.(12) is executed in order to obtain $F(T)$. Before the parametric study, the calculation of the Floquet exponent was checked by putting U_w in Eq.(2) onto 0. In this case, the Floquet exponent should be equivalent to the eigenvalue of the plane Poiseuille flow. Table 1 shows the comparison of the eigenvalues obtained in the present study with the results by Orszag[11]. It seems that the accuracy of the numerical scheme using here is sufficient.

Table 1 Comparison of the eigenvalues

	ω_r	ω_i
present	0.23753e+00	0.37397e-02
Orszag[1]	0.23752464	0.00373967

Figure 3 shows the variation of eigenvalues in a period for the case of R_e=10,000, (Ω, U_w)=(0.01,0.1) and (k_x,k_z)=(1.0,0.0). Two straight lines are correspond to the eigenvalues of the simple plane Poiseuille flow, namely non-oscillating case. It can be seen in this figure that the stable and unstable phase change place each other in a period.

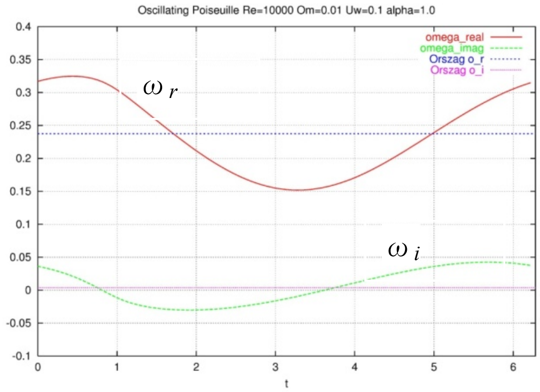

Fig.3 Variation of eigenvalues in a period for the case of Re=10,000, (Ω, U_w)=(0.01,0.1) and (k_x,k_z)=(1.0,0.0).

This investigation is liken to a quasi-steady analysis and it is difficult to find out whether this system is stable or not as the whole.

Thus, the Floquet analysis is executed in order to estimate in overall stability. Result of the parametric study is shown in Fig. 4 as a contour map on Ω-U_w plane. The white color region represents the positive area of the Floquet exponent, which corresponds to the unstable region, and the black one corresponds to the stable one. The dash-dotted lines in this figure are written by each 0.002 of the Floquet exponent, and the solid line represents zero eigenvalue, namely the neutral curve. It can be seen that the stable region exists as a deep crevasse along U_w axis. Regardless of the value of Ω, wall oscillation stabilizes the present system.

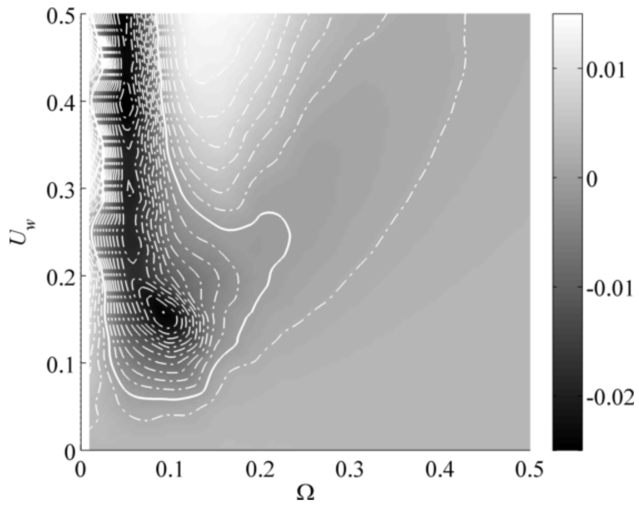

Fig. 4 Contour of the Floquet exponent. White color corresponds to the unstable region, and black to the stable one. A white solid line represents the neutral curve.

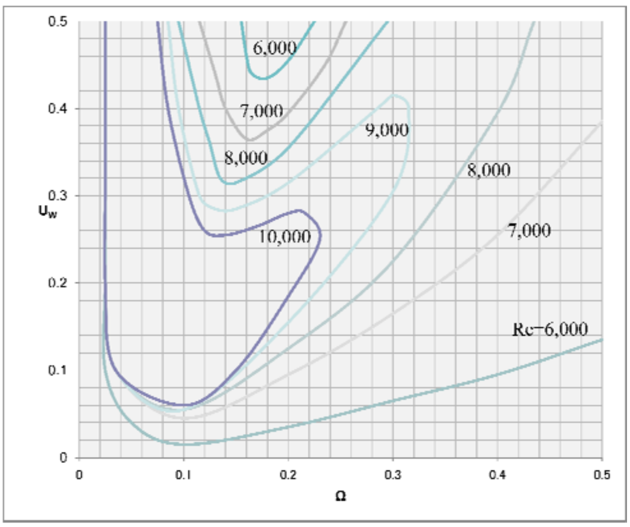

Fig. 5 Contour of the Floquet exponent. White color corresponds to the unstable region, and black to the stable one. A white solid line represents the neutral curve.

To understand the characteristics of the effect of the wall-oscillation entirely, the neutral curves for different R_e number. This result is shown in Fig. 5. A deep crevasse mentioned above still exists for all cases, and a stable valley spreads over by U_w=Ω line. It becomes clear that the stable region exists broadly in the parameter space.

4 Direct Numerical Simulation

4.1 Government Equation and Numerical Procedure

Figure 6 shows numerical space which is set as $x \in [0,4\pi]$, $y \in [0,2\pi]$, $z \in [-1,-1]$. To capture smaller structures in x direction, the resolution is increased. The number of grid in each directions are 128, 129, 64. The periodic condition is adopted in y direction.

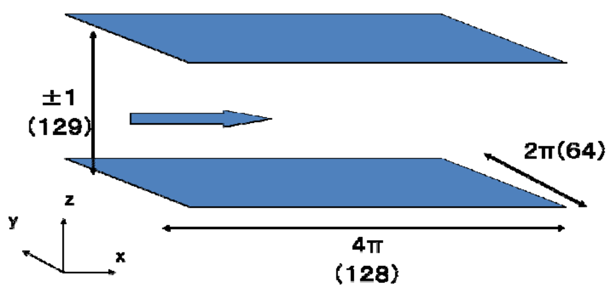

Fig. 6 Numerical space for DNS.

The flow filed is described as a superposition of the disturbance $\boldsymbol{u}$=$\boldsymbol{u}(u,v,w)$ on the basic flow $U(y,t)$. If the pressure can be written as $-2x/R_e + p$, the dimensionless equation for $\boldsymbol{u}$ is obtained from the Navier-Stokes equation,

$$\frac{\partial \boldsymbol{u}}{\partial t} + U\frac{\partial \boldsymbol{u}}{\partial x} + v\frac{\partial U}{\partial y}\boldsymbol{e}_x = -\nabla \times \boldsymbol{u} \times \boldsymbol{u} - \nabla p + \frac{1}{R_e}\nabla^2 \boldsymbol{u} \tag{18}$$

here, $\boldsymbol{e}_x$ denotes an unit vector in x the direction. The incompressible condition is,

$$\nabla \cdot \boldsymbol{u} = 0 \tag{19}$$

The velocity $\boldsymbol{u}$ is expanded by the Fourier series for x, z directions on the Chebyshev collocation points y_j.

$$\boldsymbol{u}(x, y_j, z, t) = \sum_{k_x, k_z} \boldsymbol{u}(k_x, y_j, k_z, t) \exp[i(k_x x + k_z z)] \tag{20}$$

Then, Eq.(18) is calculated by the Fourier-Chebyshev spectral method[13] for $\boldsymbol{u}(k_x,y_j,k_z,t)$ with the initial disturbances given as,

$$\boldsymbol{u}(k_x, y_j, k_z, 0) = \varepsilon \boldsymbol{q}(k_x, y_j, k_z) \tag{21}$$

where ε is a small parameter and $\boldsymbol{q}$ is a random function which satisfied the solenoidal condition. Energy norm for the Fourier modes (k_x,k_z) per unit mass is defined as the follow.

$$E(k_x, k_z) \equiv \frac{1}{4}\int_{-1}^{1} \left|\boldsymbol{u}(k_x, y, k_z)\right|^2 dy \tag{22}$$

4.2 Numerical Results

A typical results is shown in Fig.7 for the case of $(\Omega,\ U_w)$=(0.0,0.0) which corresponds to the genuine plane Poiseuille flow. The curves in this figure represent the time variation of energy for each Fourier mode $E(k_x,k_z)$. The solid lines correspond to two-dimensional disturbance, namely $E(k_x,0)$, and the dotted lines correspond to three-dimensional ones. In this calculation, the simulation has been started with the initial disturbances of order 10^{-9}, but a specific disturbance with relatively large amplitude of order 10^{-5}. This large disturbance is a Fourier mode of $E(1,0)$, which is called the Tollmien-Schlichting (TS) wave. Because it is well known that the TS mode is dominant and leads to the laminar-turbulent transition under the flow condition considered here, the large TS mode is initially added to the initial disturbance in order to save the computing time-cost. In the present study, all of the simulation examined are including this TS mode.

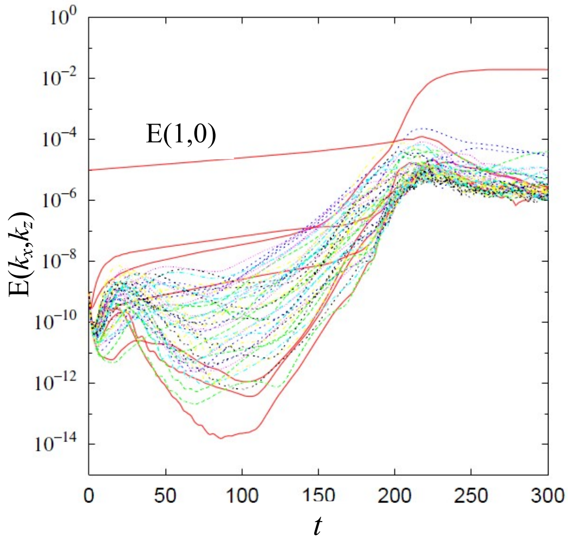

Fig. 7 Variation of energy of each Fourier mode for the case of $(\Omega,\ U_w)$=(0.0,0.0).

From this figure, it can be seen that after the transient phase the energy of the each mode develop with time and the laminar-turbulent transition occurs at about t=230 in this case.

Some results with wall-oscillation are shown Fig.8-10 for the case of $(\Omega,\ U_w)$=(0.25,0.3), (0.05,0.2), and (0.15,0.2). The result of Fig.8 seems to almost same as non-oscillating case of Fig.7 except for oscillation in the time variation of the energy for each Fourier mode. It can be easily supposed that this oscillation is caused by the oscillation of the walls. Actually, it was confirmed that the period of the oscillation appearing on the time variation of the energy coincides with that of the wall-oscillation. In Fig.9, the laminar-turbulent transition is accelerated by the wall-oscillation. In this case, it takes only about 80 non-dimensional time for the transition. On the other hand, the result of the Fig.10, the transition to turbulence is slightly delayed by the wall oscillation.

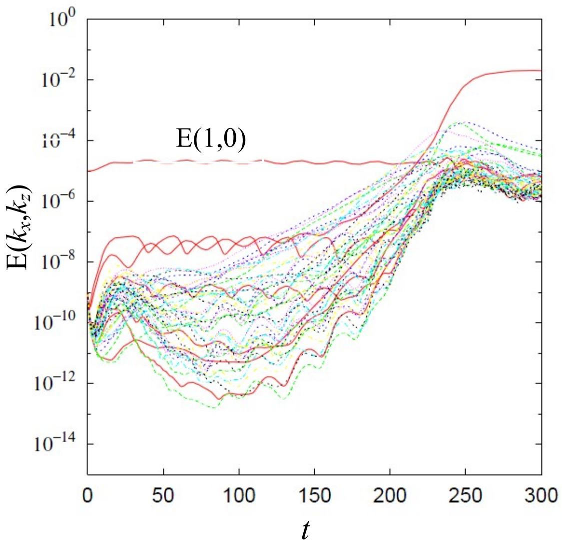

Fig. 8 Variation of energy of each Fourier mode for the case of (Ω, U_w)=(0.25,0.3).

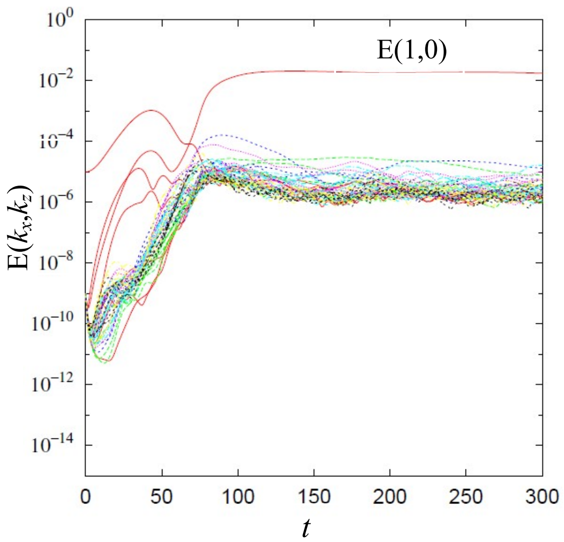

Fig. 9 Variation of energy of each Fourier mode for the case of (Ω, U_w)=(0.05,0.2).

It is found from such parametric study that the laminar-turbulent transition of the flow can roughly be grouped in three patterns depending on the wall-oscillation. Result of this parametric study is shown in Fig.11. The circles correspond to the accelerated cases, the diamonds to the decelerated, and square to the less affected cases. It seems that the accelerated cases exist in small Ω region.

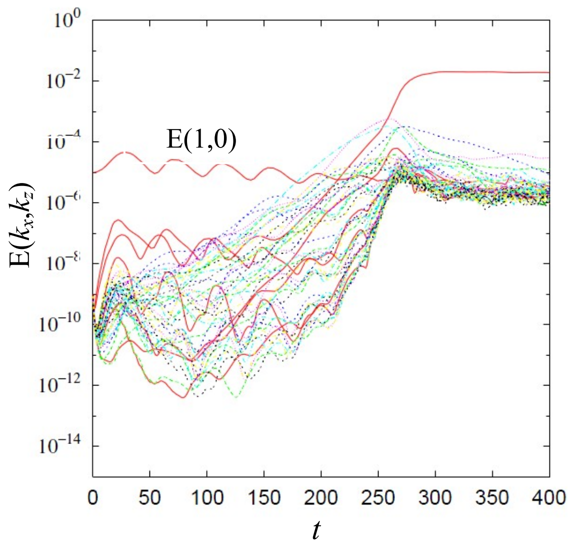

Fig. 10 Variation of energy of each Fourier mode for the case of (Ω, U_w)=(0.15,0.2).

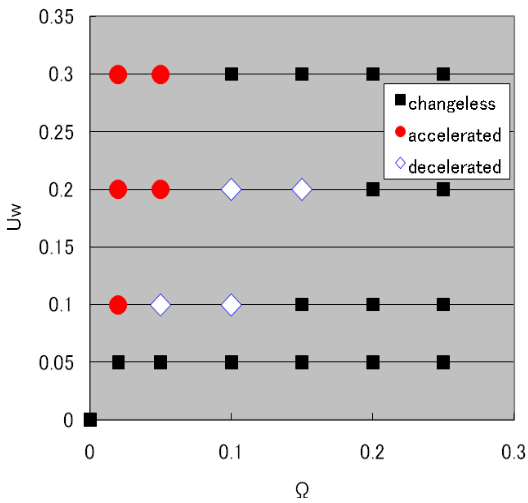

Fig. 11 Result of the parametric study.

From the comparison with Fig. 4, the decelerated region agrees well with a part of the stable region estimated by the Floquet analysis. However, even though these regions partially coincide with each other, the laminar-turbulent transition occurs at least in DNS. Actually, in the early state, the gradient of the TS mode and its higher harmonics are negative in DNS. Thus it is found that the transition is caused by nonlinearity. Furthermore, the accelerated region does not agree well. Since the thickness of the Stokes layer increases when frequency of the wall-oscillation decreases, it can be conjectured that the assumption of describing the flow by a linear combination of the plane Poiseuille flow and the Stokes layer is not suitable for small Ω values. Except for this region, these results suggest that the Floquet analysis can prospect the tendency of transition delay by watching stability of the dominant TS mode.

5 Conclusion

The present study investigates a stabilizing effect of longitudinal wall-oscillation on two dimensional channel flow by the Floquet theory. To apply this theory to the present periodic flow, a time-dependent Orr-Sommerfeld equation is discritized using the collocation points. The velocity profile needed in this analysis is calculated by superposition of the plane Poiseille flow and the Stokes layer because of the linearity of the governing equation. In this study, the Reynolds number, which is defined by maximum mean-flow velocity and a half width between the two walls, is fixed to 10,000 that corresponds to the turbulent state of usual channel flow. When the remaining two parameters, frequency and amplitude of the wall-oscillation, are changed parametrically, it is found that on the parameter space the stable region exists even under the supercritical condition. The direct numerical simulation (DNS) also carried out to validate this feature. DNS demonstrates that the transitional period to the fully turbulent state is longer or shorter compared with non-oscillating case depending on the parameters mentioned above. The comparison of the results obtained the Floquet analysis with DNS shows that the stable region in the Floquet analysis roughly coincides with the region of slow transition.

References

1) Selvarajan, S., Tulapurkara, E.G., and Vasanta Ram, V.: Stability Characteristics of Wavy Walled Channel Flows, *Phys. Fluids*, **11** (1999), pp. 579-589.
2) Floryan, J. M.: Stability of Wall-Bounded Shear Layers in the Presence of Simulated Distributed Surface roughness, *J. Fluid Mech.,* **335** (1997), pp. 29-55.
3) Floryan, J. M., Szumbarski, J., and Vasanta Ram, V.: Stability of a Flow in a Channel with Vibrating Walls, *Phys. Fluids*, **14** (2002), pp. 3927-3936.
4) Zhou, H., Martinuzzi, R. J., Khayat, R. E., Straatman, A. G., and AbuRamadan, E.: Influence of Wall Shape on Vortex Formation in Modulated Channel Flow, *Phys. Fluids*, **15**, (2003), pp.3114-3133.
5) Choi, H., Moin, P., and Kim, J.: Active Turbulence Control for Drag Reduction in Wall Bounded Flows, *J. Fluid Mech.*, 262 (1994), pp.75-110.
6) Sumitani, Y. and Kasagi, N.: Direct Numerical Simulation of Turbulent Transport with Uniform Wall Injection and Suction, *AIAA J.*, **33**, (1995), pp.1220-1228.
7) Jung, W. J., Mangiavacchi, N., and Akhavan, R.: Suppression of Turbulence in Wall-Bounded Flows by High-Frequency Spanwise Oscillations, *Phys. Fluids*, A 4 (8) (1992), pp.1605-1607.
8) Quadrio, M. and Ricco, P.: Critical Assessment of Turbulnet Drag Reduction Through Spanwise Wall Oscillation, *J. Fluid Mech.*, **521**, (2004), pp.251-271.
9) Choi, K.-S.: Near-Wall Structure of Turbulent Boundary Layer with Spanwise-Wall Oscillation, Phys. Fluids, 14 (2002), pp.2530-2542.
10) Ricco, P. and Quadrio, M.: Wall-Oscillation Conditions For Drag Reduction in Turbulent Channel Flow, *Int. J. Heat Fluid Flow*, **29** (4) (2008), pp. 891-902.
11) Orszag, S. A.: Accurate Solution of the Orr-Sommerfeld Stability Equation, *J. Fluid Mech.*, **50**, 689 (1971), pp.1441-1447.
12) Kim, J., Moin, P., and Moser, R..: Turbulence Statistics in Fully Developed Channel Flow at Low Reynolds Number, *J. Fluid Mech.*, 177 (1987), pp.133-166.
13) Canuto, C., Hussaini, M. Y., Quarteroni, A. and Zang, T. A.: *Spectral Methods in Fluid Dynamics*, Springer-Verlag, Berlin, 1988.

Copyright Statement